# Potential Toxicity of Graphene to Cell Functions *via* Disrupting Protein–Protein Interactions

**Binquan Luan,*,† Tien Huynh,† Lin Zhao,‡ and Ruhong Zhou*,†,¶,‡**

†Computational Biological Center, IBM Thomas J. Watson Research, Yorktown Heights, New York 10598, United States, ‡Institute of Quantitative Biology and Medicine, SRMP and RAD-X, Collaborative Innovation Center of Radiation Medicine of Jiangsu Higher Education Institutions, Soochow University, Suzhou 215123, China, and ¶Department of Chemistry, Columbia University, New York, New York 10027, United States

**ABSTRACT** While carbon-based nanomaterials such as graphene and carbon nanotubes (CNTs) have become popular in state-of-the-art nanotechnology, their biological safety and underlying molecular mechanism is still largely unknown. Experimental studies have been focused at the cellular level and revealed good correlations between cell's death and the application of CNTs or graphene. Using large-scale all-atom molecular dynamics simulations, we theoretically investigate the potential toxicity of graphene to a biological cell at molecular level. Simulation results show that the hydrophobic protein–protein interaction (or recognition) that is essential to biological functions can be interrupted by a graphene nanosheet. Due to the hydrophobic nature of graphene, it is energetically favorable for a graphene nanosheet to enter the hydrophobic interface of two contacting proteins, such as a dimer. The forced separation of two functional proteins can disrupt the cell's metabolism and even lead to the cell's mortality.

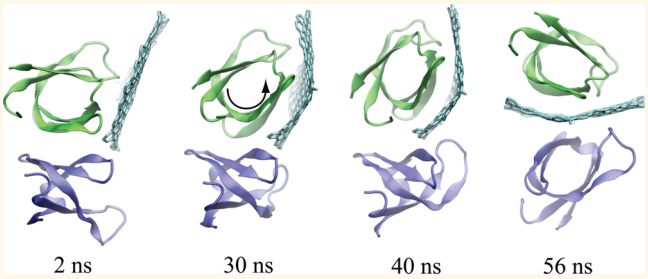


**KEYWORDS:** nanotoxicity · graphene nanosheet · protein–protein interaction

Carbon-based nanomaterials, such as a carbon nanotube (CNT) and graphene, have been extensively studied for their applications in nanotechnology, because of their mechanical stability at low dimensions,[1] well predicted surface chemistry after oxidation or functionalization,[2] favorable electronic conductivity[3] and outstanding optical properties.[4] For example, graphene has been used as a low-dimensional transparent electrode,[5] an optical probe for nanoelectromechanical system (NEMS),[6] a biological sensor,[7] a field-effect transistor,[8] and so on. Because of their potential wide applications, CNT's or graphene's nanotoxicity to a biological cell has raised serious concerns about human health. Until now, recent theoretical studies of graphitic nanomaterials have shown that a bulky ball[9] or CNT[10] can penetrate the cell membrane or be internalized through endocytosis.[11] Experimentally, it was demonstrated that CNTs can be found in cytoplasm and nucleus inside a cell.[12] Therefore, unexpected interactions between graphitic nanomaterials and biological molecules (such as DNA and protein) inside the cell can interfere with biological functions, resulting in cytotoxic effects.[13]

Toxicity of a CNT has been extensively studied theoretically, including the modeling of CNT–membrane interactions and pathways to the internalization of CNTs.[14] After the CNT's entry into a cell, biological functions can be affected by the toxic binding between the CNT and the protein or DNA. Theoretical studies also showed that a CNT can win the competitive binding over proline-rich motif ligand on the SH3 domain.[15] It is therefore expected that the function of the SH3 domain can be inhibited. Additionally, the genotoxicity of CNT to DNA was indicated in a previous study[16] by showing the wrapping of a single-stranded DNA (ssDNA) around the CNT *via* strong $\pi-\pi$ stacking. Interestingly, on the other hand, the binding of blood proteins to carbon nanotubes, which prevents CNTs from entering the cells, may reduce the cytotoxicity of a CNT.[17]

* Address correspondence to bluan@us.ibm.com, ruhong@us.ibm.com.

Received for review October 21, 2014 and accepted December 13, 2014.

**Published online December 13, 2014**
**10.1021/nn506011j**

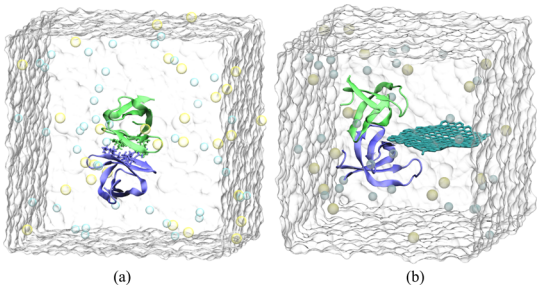


**Figure 1. Illustration of simulated systems without (a) and with (b) the presence of a graphene nanosheet. The two subunits of the protein dimer, colored in green and blue, respectively, are in the cartoon representation. Water is shown transparently; sodium and chlorine ions are, respectively, shown as yellow and cyan spheres. In (a), hydrophobic residues at the dimer interface are highlighted and drawn as connected sticks. In (b), a graphene nanosheet is placed near the protein dimer.**

The potential toxicity of graphene to biological molecules has been indicated in limited studies. For example, the strong $\pi-\pi$ stacking between the aromatic residues of a protein and graphene may cause denature of the protein.[15] Graphene nanosheets are also shown to disrupt *Escherichia coli* cell membranes through penetration and direct extraction of phospholipid molecules, thus providing a potential new class of green antibiotics.[18] Here, we investigate the potential toxicity of graphene through the interference of protein−protein interactions (PPI). In fact, proteins rarely act alone, but rather carry out their functions by various PPIs. Many biological processes in a cell, such as signal transduction and cell metabolism, are carried out through PPI. Abnormal PPI can cause the failure of a biological function and lead to many diseases (*e.g.*, cancer or Alzheimer's disease).

As a proof-of-principle study, we focus on the noncovalent PPI with a hydrophobic interface. Strong hydrophobic interactions through a matching of large hydrophobic surface area can exist in these PPI, as shown in previous theoretical studies[19] for the melittin tetramer (PDB ID: 2MLT), the 2-deoxyribose-5-phosphate aldolase from *Thermus thermophilus* HB8 (PDB ID: 1J2W) and the phosphoglucose isomerase (PDB ID: 1J3Q). The system investigated here is the C-terminal DNA-binding domain of human immunovirus-1 (HIV-1) integrase[20] that can form a dimer in solution and shows a well-defined hydrophobic interface. We performed all-atom molecular dynamics (MD) simulations to analyze the hydrophobic PPI and the separation of the dimer *via* graphene's insertion (*i.e.*, potential toxicity).

## RESULTS AND DISCUSSION

Figure 1a illustrates the simulation system of the protein dimer in a water box. The folded protein structure (PDB ID: 1QMC) resembles the one of the SH3 domain.[21] Sodium and chlorine ions were added to neutralize the simulation system and to yield the

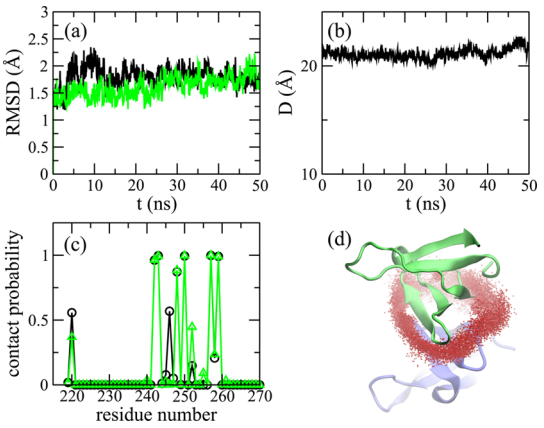


**Figure 2. Simulation of the protein dimer without the graphene nanosheet. (a) RMSDs of both monomers in the dimer. (b) Time-dependent distances between two monomers. (c) Contact probabilities of each residue in one monomer with the other monomer. (d) An illustration of the hydrophobic contact. Oxygen atoms in water molecules within 5 Å of both monomers are shown as red dots.**

concentration of the resulting electrolyte at 0.1 M. The entire simulation system measures 77.4 × 77.4 × 77.4 Å$^3$. During the 50 ns simulation, each monomer's secondary structure was stable as indicated from the root-mean-square deviations (RMSD) of the atoms in the protein backbone. RMSDs were calculated against the initial crystal structure of each monomer. After about 5 ns, the RMSDs saturate at around 1.8 Å (Figure 2a). The structures of both monomers remained stable during the rest of the 45 ns of simulation. The distance *D* between the two monomers in the dimer is defined as the length from the center of mass (COM) of one monomer to the COM of the other. From the entire 50 ns of simulation, the monomer−monomer distances stayed nearly constant and were around 21 Å, as shown in Figure 2b. This result suggests that the dimer was stable.

Figure 2c shows the probabilities of the residues being inside the contact between the two monomers. A residue of one monomer is considered to be inside the contact if any atom of that residue is within 3 Å of the other monomer. The contact probability of a residue is calculated as the ratio between the total time for the residue staying inside the contact and the entire simulation time. Six hydrophobic residues (LEU242, TRP243, ALA248, VAL250, ILE257, VAL259) show high (∼100%) probabilities to be inside the contact. These six residues are highlighted in Figure 1a. The residue ILE220 is in the flexible terminal of one monomer and can contact the other monomer from time to time. But this residue is not inside the hydrophobic contact. Two hydrophilic residues GLU246 and GLN252 that have non-zero probabilities are in the flexible turns between the neighboring beta-sheets and are located at the edge of the hydrophobic contact. The rest of the residues have zero or negligible probabilities, *i.e.*, not inside the contact (Figure 2c).

The hydrophobic contact is illustrated in Figure 2d. From the simulation trajectory, Figure 2d shows the overlap of 1000 frames (sampled every 50 ps) of water molecules (represented by red dots) within 5 Å of both monomers. Notably, no water molecule was found inside the hydrophobic contact, *i.e.*, a complete drying between the hydrophobic surfaces.[19]

Overall, Figure 2 shows that the dimer structure, as well as the secondary structure of each monomer, is stable. The protein−protein contact results from the hydrophobic interaction by six interfacial residues of each monomer. Thus, the dimer structure *via* hydrophobic interaction potentially could be broken after the insertion of graphene, which is demonstrated below.

Figure 1b illustrates the simulation system of the dimer-graphene complex with a 0.1 M NaCl electrolyte. A hexagonal graphene sheet whose one-side-surface area is 1100 Å$^2$ was placed near the hydrophobic interface of the dimer. The surfaces of the graphene sheet were parallel to the dimer interface at the beginning of the simulation. Two independent simulations (Sim-1 and Sim-2) were carried out for graphene in the putative DNA binding site of the dimer,[20] as shown in Figure 1b. In the other two independent simulations (Sim-3 and Sim-4), the graphene sheet was placed on the opposite side of the dimer (see Figure 3f).

To calculate the contact area of the dimer, we analyzed the solvent-accessible surface areas (SASA) of each monomer and the dimer complex from the simulation trajectories. Typically, the SASA is the area of a conforming surface that is ~3 Å away from an object (*e.g.*, a monomer or a dimer), *i.e.*, by rolling a water molecular around the molecular surface. Assuming that the SASAs of each monomer (labeled as "A" and "B") and the dimer complex are denoted by $s_A$, $s_B$ and $s_{AB}$, respectively, the contact area $S_{AB}$ can be written as,

$$S_{AB} = (s_A + s_B - s_{AB})/2 \quad (1)$$

Calculated from all four simulations, the time-dependent contact areas of the dimer are shown in Figure 3. Notably, $S_{AB}$ changes from a constant mean value to zero in all four simulations, indicating that the dimer structure was broken during the simulation. Depending on whether the flexible loops or terminals of one monomer are in contact with the other one, the initial contact areas fluctuate around a mean value that varies from 300 and 350 Å$^2$ in four independent simulations. Analyses from the simulation trajectories show that the graphene sheet can spontaneously enter into the dimer, as illustrated in Figure 3b−i. After the separation of the dimer by the graphene sheet, the SASA of the two monomers is simply the sum of the SASA of each monomer. Thus, as shown in Figure 3, the values of $S_{AB}$ decrease to zero for all four simulations.

Figure 3b−e illustrates the insertion process of the graphene nanosheet from the trajectory of Sim-1.

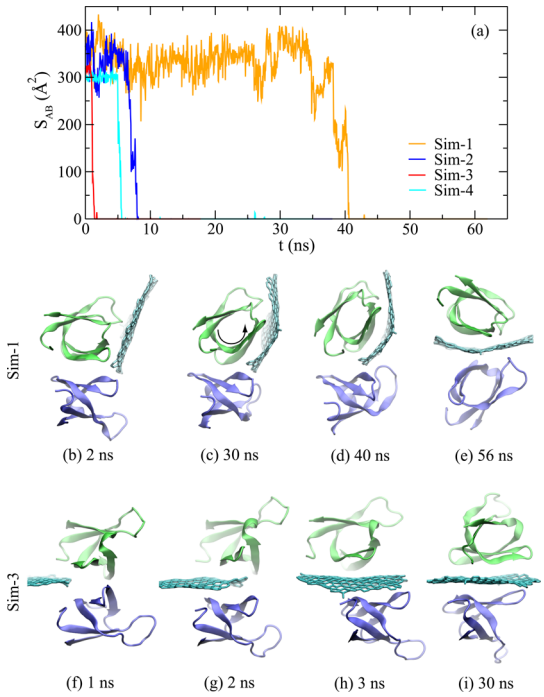


**Figure 3. Dynamics of the insertion of a graphene sheet into the dimer. (a) Time-dependent contact areas of the dimer during the insertion of a graphene sheet. (b) Snapshots of the insertion process of a graphene sheet into the dimer from the first simulation trajectory (Sim-1). (c) Snapshots of the insertion process of a graphene sheet into the dimer from the third simulation trajectory (Sim-3).**

Initially parallel and close to the dimer's interface, the graphene sheet rotated and contacted one monomer after 2 ns (Figure 3b), while one edge of the graphene sheet remained in the vicinity of the dimer interface. This process was driven by the favorable van der Waals (vdW) interaction between the protein and the graphene sheet. Because the graphene surface is hydrophobic, the energy penalty due to the unfavorable graphene−water interaction outweighs the one due to the graphene−protein interaction. Thus, typically, a protein molecule with hydrophobic residues on its surface can be adsorbed on the graphene surface, which was also shown previously.[15] After about 30 ns, the flexible graphene sheet contacted the protein conformally, *i.e.* maximizing the contact area (or reducing the unfavorable graphene−water interaction). Many hydrophilic (polar/charged) residues of the monomer, such as SER230 and ARG231 (containing hydrophobic parts), were also found inside the contact. From 30 to 40 ns, the monomer began to rotate about its barrel axis, due to the preferred hydrophobic interaction between the graphene surface and nonpolar residues at the dimer interface. Meanwhile, interfacial nonpolar residues of the other monomer began to interact with the other side the graphene sheet, similarly driven by the graphene−protein interaction that is more hydrophobic than the one between the two protein monomers. At 56 ns, the graphene sheet was fully inserted

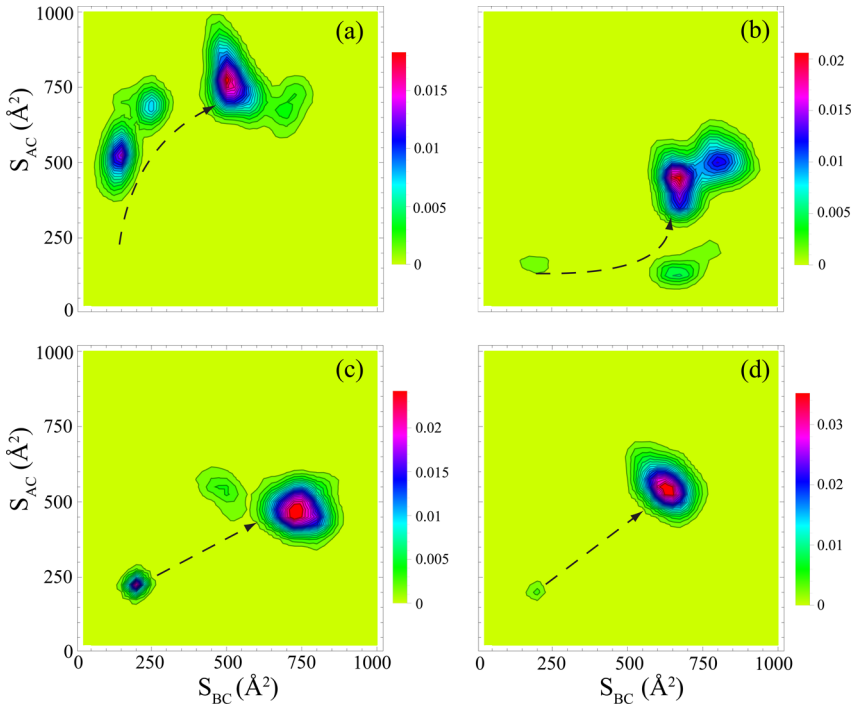


**Figure 4. Probability map of contact areas between monomers (labeled as "A" and "B") and the graphene sheet (labeled as "C"). Results of four independent simulation trajectories (Sim-1, Sim-2, Sim-3 and Sim-4) are shown in panels (a), (b), (c), and (d), respectively. An arrow in each panel shows probability changes from the beginning to the end of the simulation.**

and the dimer was separated (see movie in Supporting Information). Noticeably, the two protein monomers moved independently and the two initially perpendicular barrel axes became parallel. For a larger graphene sheet, the two monomers may not be on top of each other and separate laterally (along graphene surfaces). The independent Sim-2 showed similar insertion process of the graphene sheet.

The trajectory of Sim-3 illustrates a different insertion process of the graphene sheet (Figure 3f–i). In this simulation, the graphene sheet was placed on the opposite side of the dimer (Figure 3f), where both surfaces of the graphene sheet can be simultaneously in contact with the hydrophobic resides of both monomers. As a result, the graphene sheet entered the hydrophobic interface of the dimer very quickly (after only 1 ns) and separated the dimer completely at around 3 ns. After that, motions (rotation and translation) of the two monomers on the graphene's surfaces are relatively independent. The insertion process only took slightly longer (~5 ns) in Sim-4 and the dynamic process is similar to that of Sim-3.

Overall, all simulations demonstrate the fast insertion of the graphene sheet into the dimer, which can be attributed by the following two reasons. First, the unfavorable interaction between graphene and water leads to graphene's contacts with the dimer. In Sim-1 and Sim-2, the graphene sheet contacted the noninterfacial part (containing hydrophilic residues) of the dimer. The following entry into the dimer interface is driven by the interaction with hydrophobic residues. While in Sim-3 and Sim-4, the graphene sheet contacted the interfacial part of the dimer, *i.e.* an direct insertion. Second, interfacial interactions between hydrophobic residues in the dimer yielded to the energetically more favorable (see below) interaction between hydrophobic residues and the graphene sheet. Thus, the separation (or unzipping) process of contacting hydrophobic residues at the graphene edge is very fast (in a few ns).

From the analyses of the MD trajectories, the insertion process can be illustrated from the probabilities of the contact areas ($S_{AC}$ and $S_{BC}$), as shown in Figure 4. When the graphene sheet is at the edge of the protein–protein contact, the contact area between the graphene sheet and one monomer is about 200 Å$^2$. Figure 4a shows that $S_{AC}$ was increased to about 500 Å$^2$, indicating that the graphene sheet preferably contacted monomer A before the insertion. Once the insertion occurred, both $S_{AC}$ and $S_{BC}$ increased. Figure 4a shows that the most possible values for $S_{AC}$ and $S_{BC}$ are around 750 and 500 Å$^2$. The value of $S_{AC}$ is larger because the flexible graphene sheet was bent toward monomer A (see Figure 3e). The arrow in Figure 4a shows the time-dependent change of probabilities. From the trajectory of Sim-2, Figure 4b shows that the graphene sheet contacted monomer B first and in the final simulated state the graphene sheet was bent toward monomer B (because $S_{BC} > S_{AC}$).

Corresponding to the direct insertion of the graphene sheet into the dimer, as shown in Figure 3f,g, the probability maps (Figure 4c,d) illustrates the simultaneous

increase of $S_{AC}$ and $S_{BC}$. After the insertion, the mean values of $S_{AC}$ and $S_{BC}$ were different due to the bending of the graphene sheet toward one of the monomers. These dynamic processes of the graphene's insertion were observed in two independent simulations (Sim-3 and Sim-4).

Two different mechanisms of the graphene's insertion, observed in simulations, are related to the surface geometry of the dimer. The "wrapping"-assisted mechanism (shown in Sim-1 and Sim-2) results from the placement of the graphene sheet at the concave surface (putative DNA-binding site) of the dimer. Thus, before or during the insertion of the graphene sheet, it is likely that the graphene sheet contacts one monoer. Likewise, the direct-insertion mechanism (shown in Sim-3 and Sim-4) is due to the convex surface of the dimer where the graphene sheet is placed. Thus, the graphene sheet is less likely to contact each monomer.

Since the graphene surface is highly hydrophobic, it is energetically unfavorable for the graphene sheet to be exposed to water. Inside the dimer, the protein−protein contact has a hydrophobic interface. Thus, to minimize the potential energy of the graphene sheet, it is preferable for the graphene sheet to enter the hydrophobic interface of the dimer. As for the monomers, each monomer may interact with the graphene sheet more hydrophobically, *i.e.*, reducing the vdW potential energy of each monomer too after the graphene's insertion. To demonstrate that the insertion process is driven by the potential minimization, we calculated the time-dependent van der Waals energies: $E_{AB}$ between monomer A and monomer B (black line in Figure 5), $E_{AC}$ between the graphene sheet and monomer A (orange line in Figure 5), as well as $E_{BC}$ between the graphene sheet and monomer B (blue line in Figure 5).

As described above for the insertion process in Sim-1, before the insertion, the graphene sheet contacted monomer A first (Figure 3b). Correspondingly, the vdW energy between the graphene sheet and monomer A was reduced by about 60 kcal/mol (orange line in Figure 5), while the van der Waals energy between the graphene sheet and monomer B remained constant (blue line in Figure 5) . Similarly, without the insertion of the graphene sheet, the vdW energy between the two monomers were constant (black line in Figure 5). The insertion process finished at around 42 ns. After that, the vdW energy for the dimer increased about 30 kcal/mol. Meanwhile, vdW energies between the graphene sheet and monomers decreased about 60 kcal/mol for monomer B and 100 kcal/mol for monomer A. Again, the energy difference results from the bending of the graphene sheet toward monomer A. Overall, the insertion process lowered the van der Waals potential of the graphene−dimer complex by 130 kcal/mol. Therefore, with an insertion distance of ~1 nm, an averaged driving force resulting from the strong hydrophobic interaction is estimated to be around 1 nN, during the graphene's insertion process.

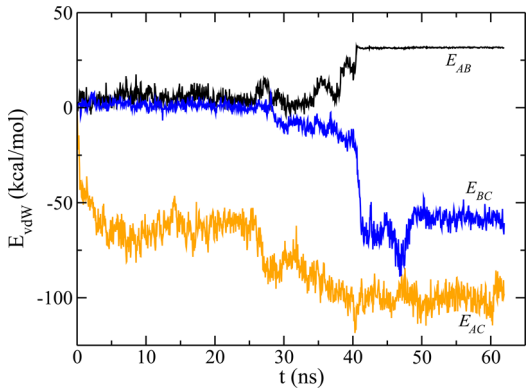


**Figure 5. Time-dependent van der Waals interactions between monomers in the dimer (black), between monomer A and the graphene sheet (orange), and between the monomer B and the graphene sheet (blue). These results were obtained from the trajectory analyses of Sim-1.**

Besides the stronger interaction strength between the graphene sheet and each hydrophobic residue, a graphene surface is atomically flat and can yield a larger contact area with a protein monomer. The later contains a hydrophobic surface that has a typical roughness of $\sigma$ (several angstroms). The PPI inside a dimer is from the contact between two rough and incommensurate surfaces.[22] From the point of view of contact mechanics, this contact is equivalent to the contact between a flat and an even rougher ($\sqrt{2}\sigma$) surface. Therefore, the atomic-scale contact area inside the PPI is normally less than that from the contact between a flat graphene surface and a protein surface. Consequently, the van der Waals interaction that is proportional to the contact area is typically stronger between graphene and one monomer than between two monomers. Thus, it is energetically favorable for graphene to separate the hydrophobic PPI. For the case studied here, after the separation, each monomer is in contact with the graphene, which further reduces the interaction potential by two times.

## CONCLUSIONS

In summary, using MD simulations, we investigate the possible toxicity of graphene (or the pristine part of the graphene oxide) that can interfere the PPI. Along with previous MD studies,[23] this work demonstrates that atomistic simulations, providing detailed nanoscopic interactions between molecules, can not only help to understand graphene's toxicity revealed in experiments but also predict new toxical phenomena. Our simulation results show that, after the graphene's insertion into the protein−protein interface, the PPI *via* the hydrophobic interaction can be destabilized and the complex of the proteins can be broken. Because of the flatness and the strong hydrophobicity of graphene, the vdW potential energy, between graphene and

proteins is significantly reduced after the insertion. This indicates that once the graphene is inside a cell it is likely to break some PPIs and consequently cause the functional failure and/or even the mortality of a cell. This study of graphene's insertion into a hydrophobic interface indicates that energetically the graphene sheet may not interfere the PPIs with hydrophilic interactions as much.

Experimentally, it may be challenging but possible to conduct an *in vitro* study to confirm the graphene's interference with PPIs by identifying the binding sites. The binding of the protein and graphene needs to be at or near the dimer interface in order to confirm that the dimer is indeed being cut into monomers. First, UV and UV−vis circular dichroism (CD) methods could be used to investigate specific changes in the secondary structures and charge-transfer transitions in the protein dimer before and after the graphene's insertion. Second, the presence of a graphene sheet at the dimer interface and the specific binding sites can be identified by nucleation using nuclear magnetic resonance (NMR). A two-dimensional $^{1}H,^{15}N$ heteronuclear singular quantum correlation (HSQC) spectrum[24] can identify changes in chemical shift of NH groups in the protein backbone that are close to the graphene. Thus, the graphene's insertion can be verified if all identified NH groups are from hydrophobic residues at the protein−protein interface. Third, by using H/D exchange combined with proteolysis-mass spectrometry (MS), the conformational stability and orientation of a protein bound to a silica nanoparticle (or a graphene nanosheet) was determined.[25,26] A similar approach might be applicable to the graphene nanosheet here, which will again reveal the binding site. Lastly, by conducting functional experiments *in vitro* (e.g., the binding of the HIV-IN and a host DNA) with and without graphene nanosheets, the interaction between graphene and PPIs might be inferred.

Given the significant amount of efforts in the field of graphene research, there is no doubt that graphene will soon be widely used in nanotechnology. How to reduce grephene's toxicity (*via* functionaliztion) or increase its biological safety should be an integral part of the graphene research.

## METHODS

All MD simulations were carried out on the IBM BlueGene supercomputer, using the software package NAMD2.9.[27] The CHARMM force field[28] was applied to the protein; the standard force field for ions[29] was used for NaCl; the TIP3P mode[30,31] was chosen for water and the force field for graphene (Figure 1b) was described in the previous study.[18] We applied periodic boundary conditions in all three dimensions. Long-range Coulomb interactions are computed using particle-mesh Ewald (PME) full electrostatics over a 64 × 64 × 64 grid while the van der Waals interactions between the atoms were calculated using a smooth (10−12 Å) cutoff. After the equilibration of the simulation system at 1 bar and at 300 K (Nosé-Hoover Langevin piston pressure control[32]), production runs were carried out in the NVT ensemble.

*Conflict of Interest:* The authors declare no competing financial interest.

*Supporting Information Available:* The movie showing the MD trajectory of graphene's insertion into the dimer. This material is available free of charge *via* the Internet at http://pubs.acs.org.

## REFERENCES AND NOTES


1. Lee, C.; Wei, X.; Kysar, J. W.; Hone, J. Measurement of the Elastic Properties and Intrinsic Strength of Monolayer Graphene. *Science* **2008**, *321*, 385–388.
2. Ramanathan, T.; Abdala, A.; Stankovich, S.; Dikin, D.; Herrera-Alonso, M.; Piner, R.; Adamson, D.; Schniepp, H.; Chen, X.; Ruoff, R.; *et al.* Functionalized Graphene Sheets for Polymer Nanocomposites. *Nat. Nanotechnol.* **2008**, *3*, 327–331.
3. Neto, A. C.; Guinea, F.; Peres, N.; Novoselov, K. S.; Geim, A. K. The Electronic Properties of Graphene. *Rev. Mod. Phys.* **2009**, *81*, 109.
4. Nair, R.; Blake, P.; Grigorenko, A.; Novoselov, K.; Booth, T.; Stauber, T.; Peres, N.; Geim, A. Fine Structure Constant Defines Visual Transparency of Graphene. *Science* **2008**, *320*, 1308–1308.
5. Kim, K. S.; Zhao, Y.; Jang, H.; Lee, S. Y.; Kim, J. M.; Kim, K. S.; Ahn, J.-H.; Kim, P.; Choi, J.-Y.; Hong, B. H. Large-Scale Pattern Growth of Graphene Films for Stretchable Transparent Electrodes. *Nature* **2009**, *457*, 706–710.
6. Reserbat-Plantey, A.; Marty, L.; Arcizet, O.; Bendiab, N.; Bouchiat, V. A Local Optical Probe for Measuring Motion and Stress in a Nanoelectromechanical System. *Nat. Nanotechnol.* **2012**, *7*, 151–155.
7. Min, S. K.; Kim, W. Y.; Cho, Y.; Kim, K. S. Fast DNA Sequencing with a Graphene-Based Nanochannel Device. *Nat. Nanotechnol.* **2011**, *6*, 162–165.
8. Schwierz, F. Graphene Transistors. *Nat. Nanotechnol.* **2010**, *5*, 487–496.
9. Wong-Ekkabut, J.; Baoukina, S.; Triampo, W.; Tang, I.-M.; Tieleman, D. P.; Monticelli, L. Computer Simulation Study of Fullerene Translocation through Lipid Membranes. *Nat. Nanotechnol.* **2008**, *3*, 363–368.
10. Wallace, E. J.; Sansom, M. S. Blocking of Carbon Nanotube Based Nanoinjectors by Lipids: A simulation study. *Nano Lett.* **2008**, *8*, 2751–2756.
11. Shi, X.; von Dem Bussche, A.; Hurt, R. H.; Kane, A. B.; Gao, H. Cell Entry of One-Dimensional Nanomaterials Occurs by Tip Recognition and Rotation. *Nat. Nanotechnol.* **2011**, *6*, 714–719.
12. Porter, A. E.; Gass, M.; Muller, K.; Skepper, J. N.; Midgley, P. A.; Welland, M. Direct Imaging of Single-Walled Carbon Nanotubes in Cells. *Nat. Nanotechnol.* **2007**, *2*, 713–717.
13. Zhang, Y.; Ali, S. F.; Dervishi, E.; Xu, Y.; Li, Z.; Casciano, D.; Biris, A. S. Cytotoxicity Effects of Graphene and Single-Wall Carbon Nanotubes in Neural Phaeochromocytoma-Derived PC12 Cells. *ACS Nano* **2010**, *4*, 3181–3186.
14. Lelimousin, M.; Sansom, M. S. Membrane Perturbation by Carbon Nanotube Insertion: Pathways to Internalization. *Small* **2013**, *9*, 3639–3646.
15. Zuo, G.; Zhou, X.; Huang, Q.; Fang, H.; Zhou, R. Adsorption of Villin Headpiece onto Graphene, Carbon Nanotube, and C60: Effect of Contacting Surface Curvatures on Binding Affinity. *J. Phys. Chem. C* **2011**, *115*, 23323–23328.
16. Zheng, M.; Jagota, A.; Semke, E.; Diner, B.; McLean, R.; Lustig, S.; Richardson, R.; Tassi, N. DNA-Assisted Dispersion and Separation of Carbon Nanotubes. *Nat. Mater.* **2003**, *2*, 338–342.
17. Ge, C.; Du, J.; Zhao, L.; Wang, L.; Liu, Y.; Li, D.; Yang, Y.; Zhou, R.; Zhao, Y.; Chai, Z.; *et al.* Binding of Blood Proteins to

Carbon Nanotubes Reduces Cytotoxicity. *Proc. Natl. Acad. Sci. U.S.A.* **2011**, *108*, 16968–16973.
18. Tu, Y.; Lv, M.; Xiu, P.; Huynh, T.; Zhang, M.; Castelli, M.; Liu, Z.; Huang, Q.; Fan, C.; Fang, H.; *et al.* Destructive Extraction of Phospholipids from Escherichia Coli Membranes by Graphene Nanosheets. *Nature Nanotechnol.* **2013**, *8*, 594–601.
19. Hua, L.; Huang, X.; Liu, P.; Zhou, R.; Berne, B. J. Nanoscale Dewetting Transition in Protein Complex Folding. *J. Phys. Chem. B* **2007**, *111*, 9069–9077.
20. Eijkelenboom, A. P.; Sprangers, R.; Hård, K.; Puras Lutzke, R. A.; Plasterk, R. H.; Boelens, R.; Kaptein, R. Refined Solution Structure of the C-Terminal DNA-Binding Domain of Human Immunovirus-1 Integrase. *Proteins: Struct., Funct., and Bioinfo.* **1999**, *36*, 556–564.
21. Eijkelenboom, A. P.; Lutzke, R. A. P.; Boelens, R.; Plasterk, R. H.; Kaptein, R.; Hård, K. The DNA-Binding Domain of HIV-1 Integrase Has an SH3-like Fold. *Nat. Struct. Mol. Biol.* **1995**, *2*, 807–810.
22. Luan, B.; Robbins, M. O. The Breakdown of Continuum Models for Mechanical Contacts. *Nature* **2005**, *435*, 929–932.
23. Zhou, R.; Gao, H. Cytotoxicity of Graphene: Recent Advances and Future Perspective. *Wiley Interdiscip. Rev. Nanomed. Nanobiotechnol.* **2014**, *6*, 452–474.
24. Calvaresi, M.; Arnesano, F.; Bonacchi, S.; Bottoni, A.; Calò, V.; Conte, S.; Falini, G.; Fermani, S.; Losacco, M.; Montalti, M.; *et al.* C60@ Lysozyme: Direct Observation by Nuclear Magnetic Resonance of a 1:1 Fullerene Protein Adduct. *ACS Nano* **2014**, *8*, 1871–1877.
25. Buijs, J.; Ramström, M.; Danfelter, M.; Larsericsdotter, H.; Håkansson, P.; Oscarsson, S. Localized Changes in the Structural Stability of Myoglobin upon Adsorption onto Silica Particles, as Studied with Hydrogen/Deuterium Exchange Mass Spectrometry. *J. Colloid Interface Sci.* **2003**, *263*, 441–448.
26. Shrivastava, S.; Nuffer, J. H.; Siegel, R. W.; Dordick, J. S. Position-Specific Chemical Modification and Quantitative Proteomics Disclose Protein Orientation Adsorbed on Silica Nanoparticles. *Nano Letts* **2012**, *12*, 1583–1587.
27. Phillips, J. C.; Braun, R.; Wang, W.; Gumbart, J.; Tajkhorshid, E.; Villa, E.; Chipot, C.; Skeel, R. D.; Kale, L.; Schulten, K. Scalable Molecular Dynamics with NAMD. *J. Comput. Chem.* **2005**, *26*, 1781.
28. MacKerell, A. D.; Bashford, D.; Bellott, M.; Dunbrack, R. L.; Evanseck, J. D.; Field, M. J.; Fischer, S.; Gao, J.; Guo, H.; Ha, S.; *et al.* All-Atom Empirical Potential for Molecular Modeling and Dynamics Studies of Proteins. *J. Phys. Chem. B* **1998**, *102*, 3586–3616.
29. Beglov, D.; Roux, B. Finite Representation of an Infinite Bulk System: Solvent Boundary Potential for Computer Simulations. *J. Chem. Phys.* **1994**, *100*, 9050–9063.
30. Jorgensen, W. L.; Chandrasekhar, J.; Madura, J. D.; Impey, R. W.; Klein, M. L. Comparison of Simple Potential Functions for Simulating Liquid Water. *J. Chem. Phys.* **1983**, *79*, 926–935.
31. Neria, E.; Fischer, S.; Karplus, M. Simulation of Activation Free Energies in Molecular Systems. *J. Chem. Phys.* **1996**, *105*, 1902.
32. Martyna, G. J.; Tobias, D. J.; Klein, M. L. Constant Pressure Molecular Dynamics Algorithms. *J. Chem. Phys.* **1994**, *101*, 4177–4189.